Seminars in Dialysis

ASDIN

Investigation

Influence of Temporal Variation in Wall Shear Stress on Intima-Media Thickening in Arteriovenous Fistulae

Ehsan Rajabi-Jagahrgh,*[1] Mahesh K. Krishnamoorthy,*†[1] Yang Wang,† Ann Choe,‡ Prabir Roy-Chaudhury,†§¶[2] and Rupak K. Banerjee*[2]

*Mechanical Engineering Program, School of Dynamic Systems, University of Cincinnati, Cincinnati, OH, †Dialysis Vascular Access Research Group, Division of Nephrology and Hypertension, University of Cincinnati, Cincinnati, OH, ‡Department of Radiology, Division of Nephrology and Hypertension, University of Cincinnati, Cincinnati, OH, §Department of Internal Medicine, Division of Nephrology and Hypertension, University of Cincinnati, Cincinnati, OH, and ¶Cincinnati Veterans Administration Medical Center, Cincinnati, OH

ABSTRACT

Arteriovenous fistula (AVF) failure is mainly due to venous stenosis characterized by significant amount of intima-media thickening (IMT), probably in the presence of negative (inward) remodeling. Our *hypothesis* is that the longitudinal changes in wall shear stress (WSS) within different configurations of AVF can influence remodeling factors (changes in luminal diameter (ΔD_h) and IMT) during its maturation process. D_h is an equivalent diameter for a noncircular conduit. A total of six AVFs with curved (C-AVF; $n = 3$) and straight (S-AVF; $n = 3$) configurations were created between the femoral artery and vein of three pigs, bilaterally. CT scans and ultrasounds were utilized to calculate local WSS at 2D (D: days), 7D, and 28D postsurgery. For each AVF, IMT was measured at four regions along the vein using morphometric analyses. At these regions, repeated measurements of WSS and luminal diameter of each AVF were obtained over time. The ΔD_h between 7D and 28D was significantly larger for C-AVF than for S-AVF (2.27 ± 0.67 mm vs. 0.02 ± 0.55 mm; $p < 0.05$). Also, at 28D the amount of IMT in C-AVF (77.46 ± 7.10 units) was significantly greater ($p < 0.05$) when compared with S-AVF (53.71 ± 8.23 units). These structural changes were accompanied by significantly different gradients of WSS over time (τ') for C-AVF (-0.56 ± 0.60 dyne/cm^2/day) in comparison with S-AVF (0.71 ± 0.39 dyne/cm^2/day). Negative τ' for C-AVF corresponded to reduction in WSS level over time resulting in a physiological level of WSS at 28D (4.08 ± 5.08 dyne/cm^2). In contrast, a positive τ' for S-AVF was associated with the increase in WSS levels over time causing high levels of WSS at 28D (36.68 ± 5.32 dyne/cm^2). The decrease in WSS levels for the C-AVF over time was associated with outward remodeling of the venous wall (favorable to maturation). In contrast, for S-AVF, the increase in WSS levels over time was associated with inward remodeling and subsequently, venous stenosis. Thus, temporal gradients of WSS, which could be altered by the surgical configuration of AVF, may provide important information on the remodeling behavior of AVFs. Identification of an optimal AVF configuration, which results in a temporal decrease in WSS and an outward remodeling of the venous wall, may reduce AVF maturation failure.

Arteriovenous fistulae (AVF) in response to the chronic changes in hemodynamic milieu alter its luminal diameter and wall structure, a process also known as remodeling (1,2). Arterial remodeling in AVFs is mainly characterized by dilation and intima-media hypertrophy (outward hypertrophic remodeling) (2). However, remodeling in the venous segment of the AVF may be accompanied by aggressive intima-media thickening (IMT) and reduction in luminal diameter (inward hypertrophic remodeling). This can result in the formation of venous stenosis, which is the major cause of AVF failure (3–7). Thus, study of the parameters that affect the direction and scale of remodeling in AVFs is of great clinical importance.

Among all possible factors, marked increase in flow rate is the key hemodynamic stimulus that contributes to structural changes in venous wall in AVFs (8–13). Chronic increase in blood flow is accompanied by altered wall shear stress (WSS) in AVFs, which, over time, can result in formation of an aggressive IMT. Thus, remodeling is a dynamic process, and a proper understanding of this phenomenon cannot be achieved without studying the longitudinal effects of

Address correspondence to: Rupak K. Banerjee, Professor, Mechanical Engineering Program, School of Dynamic Systems, 593 Rhodes Hall, University of Cincinnati, Cincinnati, OH 45221-0072, or e-mail: rupak.banerjee@uc.edu.

[1]Ehsan Rajabi-Jaghargh and Mahesh K. Krishnamoorthy have contributed equally to this paper.

[2]Rupak Banerjee and Prabir Roy-Chaudhury have contributed equally to this paper.

Seminars in Dialysis—2012
DOI: 10.1111/sdi.12045

hemodynamic parameters, specifically WSS. In general, it has been found that low WSS contributes to formation of atherosclerotic lesions and consequently, increase in the amount of IMT, while higher levels of WSS are believed to result in endothelial cell survival and limited IMT (8,14–17). Despite all this work, not much is known about the effect of hemodynamic changes on venous remodeling in AVFs. Also, it should be mentioned that although we considered flow to be the primary effector of venous remodeling and IMT, pressure can also play a role in structural remodeling of AVFs (18).

In our recent studies (9,19), we showed that different surgical configurations of AVFs can induce variable levels of WSS over time. A decrease in WSS levels over time was shown to result in venous' dilation, while an increase in WSS levels was accompanied by minimal changes in venous' luminal area (19). Also, we have shown that different surgical configurations of AVFs can have a significant effect on the venous flow rate (20). Our *hypothesis* in this study is that distinct temporal patterns of WSS within different surgical configurations of AVFs can influence changes in both luminal diameter and IMT in the venous segment. Accordingly, our specific *aims* are two-fold: 1) assessing the remodeling process based on the direction of venous wall thickening in conjunction with the changes in luminal diameter of AVFs and 2) correlating the effect of the temporal gradient of WSS on IMT in the venous segment of AVFs. We believe that exploring the longitudinal effects of hemodynamic parameters such as WSS on the anatomical (change in luminal diameter) and histological endpoints (IMT) will improve our understanding of AVF failure and also lead to further research, providing better insights to minimize the clinical complications of AVF. This study represents the first attempts to correlate the hemodynamic factors such as longitudinal changes in WSS with combined anatomical and histological endpoints in AVFs.

Methods

Surgical Configuration of AVF

AVFs with curved (C-AVF) and straight (S-AVF) configurations were created between the femoral artery and vein, bilaterally (Figs 1A and 1B). A total of six AVFs (three C-AVF and three S-AVF) were created in three animals.

Anatomical and Flow Measurements, and Numerical Analysis

To obtain the specific geometry of AVFs at the different postsurgery time points, standard CT angiography techniques were used. In brief, DICOMM images were acquired using a CT scanner (Siemens Medical Systems, Florsheim, Germany) with a resolution of 512×512, pixel spacing of 0.6 mm, exposure time of 375 ms, and slice thickness of 2 mm. The stack of these DICOMM images from the CT scans was used to reconstruct the 3D geometry of AVFs using image processing techniques (MIMICS 13.1, Materialise Inc, USA). Color Doppler ultrasound (ATL HDI 5000) was utilized to record the instantaneous velocity pulses at all the postsurgery time points from which the velocity pulses, averaged over three measurements, were obtained. For pig #1, these measurements were performed at 2D (D: days) and 7D postsurgery only, as this animal was sacrificed at 7D to obtain histological information at an early postsurgery time point. However, for pigs #2 and #3, additional measurements were performed at 28D postsurgery, and animals were then sacrificed at this same time point. Furthermore, computational fluid dynamic (CFD) analysis was conducted to obtain the specific flow profile of each AVF over time. In brief, an unstructured grid was generated for the reconstructed geometry of the AVF in Gambit software (ver. 6.3.2 ANSYS Inc, USA). FLUENT software (ver. 6.3 ANSYS Inc, USA) was then employed to calculate the specific flow profile for each AVF. In the CFD analysis, flow data from ultrasound measurements was applied as the boundary conditions in the proximal and distal arteries, while the stress-free boundary condition was used at the outflow vein. A detailed description of the methodologies used for the CFD analyses is provided in previous publications by our group (9,21).

Mapping Ex Vivo and In Vivo Data

On the day of surgery, radiopaque markers (white-blue threads) as shown in Figs 1A and 1B were attached to the venous segment of AVFs in conjunction with the tying off of venous tributaries using fine sutures. These markers were used as a reference for the histological analysis. After the pigs were sacrificed, AVFs were dissected out to remove surrounding fibrous tissue, fixed in formalin for 24 hours, and then embedded in paraffin (Figs 1C and 1D). For all AVFs, a reference line (Figs 1C and 1D) was drawn along the outer curvature from the venous anastomosis to the end of the venous segment. The venous segment was then cut along this line into six 4 mm blocks (Blocks A–F). To account for the shrinkage of tissue during the paraffin-embedding process, a shrinkage factor, defined as the ratio of AVF lengths before and after the embedding process, was measured ($=1.41 \pm 0.15$) and was then used to back-calculate the positions of the CT scan regions (in vivo location) associated with specific paraffin blocks. This resulted in in vivo blocks being located at approximately 5 mm increments from the anastomosis as shown in Fig 2 for a C-AVF and S-AVF.

Histology and Morphometric Analysis

Paraffin blocks were sliced into 4 μm sections. These sections were stained with hematoxylin and eosin (H and E) as shown in Figs 3A and 3B for block B of C-AVF and S-AVF of a 28D pig. The area enclosed by the solid green line specifies the luminal area, while the dashed blue line encloses the intima-media thickening. Details of the morphometric technique using Image J software (1.35P, NIH) have been provided in our earlier publications (5,22). In brief, the center of each histology section was identified in Image J software. Furthermore,

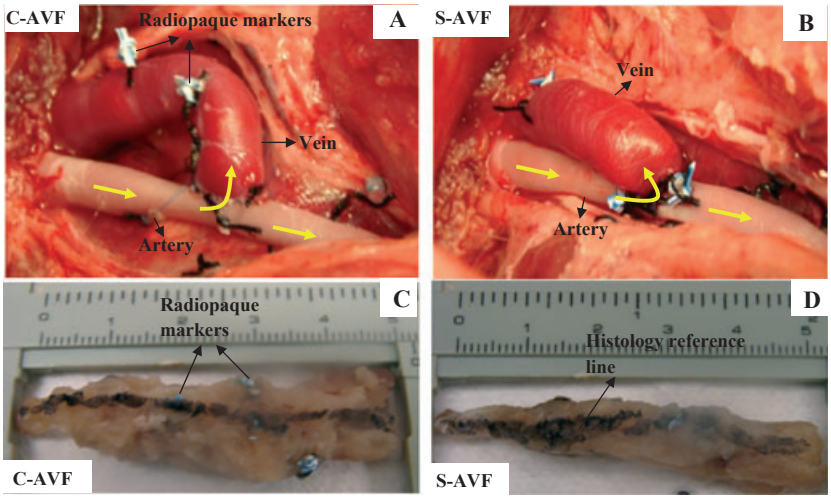

FIG. 1. Surgical configurations of (A) C-AVF and (B) S-AVF at the day of surgery. Arrows show the flow direction. The white-blue threads show the radiopaque markers sutured to the venous segments at the day of surgery. Paraffin-embedded samples for (C) C-AVF and (D) S-AVF are also shown. In addition, the reference lines (C and D) for histology were drawn from the first marker at the vicinity of anastomosis all through the vein. Note: Only some of the markers are specified with arrows to keep the clarity of the pictures.

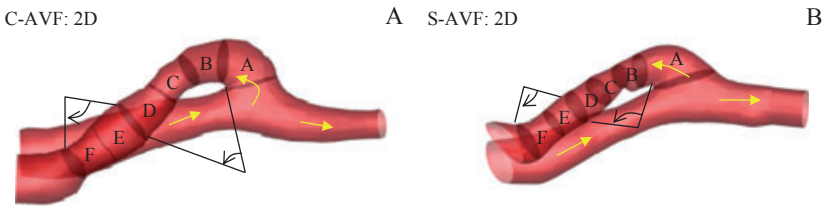

FIG. 2. Reconstructed geometries of (A) C-AVF and (B) S-AVF at 2D postsurgery. The 5 mm in vivo blocks, which correspond to the 4 mm ex vivo histology blocks, are shown along the venous segments. Note: bends sweep angles reverese after block D.

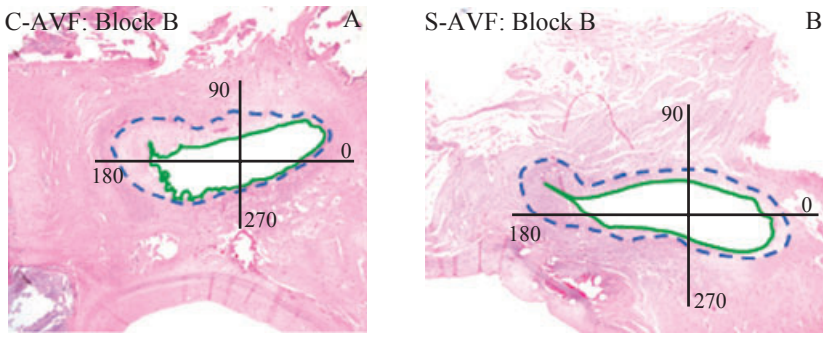

FIG. 3. Histology sections in block B of (A) C-AVF and (B) S-AVF of a 28D pig stained with hematoxylin and eosin (H and E). Area enclosed by solid green line specifies luminal area, while intima-media area is enclosed by a dashed blue line.

as shown in Fig. 3, each section was divided into 90° quadrants and subsequently, IMT was obtained by measuring the length between the lumen and the outer border of the region of intima-media thickness. Thus, four IMT values were obtained for each section, and the mean of these IMT measurements was considered to be the average thickness of the corresponding block.

Wall Shear Stress (WSS) Measurements

Within each in vivo block (Fig. 2), four cross-sections were created normal to the venous centerline. Axial time-averaged WSS at each of these cross-sections was obtained through dot product of unit normal vector of that section with time-averaged WSS (WSS averaged over the cardiac cycle). Then, these WSS values were averaged over each cross-section to obtain the spatial and time-averaged axial WSS. For simplicity, *the spatial and time-averaged axial WSS is referred to as WSS*. It should be noted that for each block, only one histology section was available. Therefore, in our analysis, the average thickness from the histology sections at each block was correlated with the average WSS over the entire block.

Furthermore, it is noteworthy that the venous segment of both C-AVF and S-AVF (Figs 2A and 2B)

was comprised of two consecutive bends with reversed curvatures. The first bend covers blocks A–D, while the second bend contains blocks E and F. As the curvature reverses in block E, new secondary flows will form that oppose the upstream vortices. These opposing vortices gradually reverse the flow field at the site of the second bend and change the location of the maximum flow zone and consequently, WSS patterns. This results in a transition region between two bends that can prolong for different distances along the second bend (23,24). Thus, blocks E and F were excluded from our analysis as they were located in the transition region between the two bends.

Statistical Analysis

Effect of WSS on IMT was statistically assessed using a random-effects model. For each AVF, WSS was measured at four cross-sections within each of the four histology blocks over time and correlated with the corresponding IMT data. Table 1 represents the matrix of data for this study. It can be seen that each hemodynamic data point involved CT scan, ultrasound measurements, and CFD analysis, while IMT was obtained through a morphometric analysis. Tukey's test was performed to ascertain the significance of differences among the two configurations. A value of $p < 0.05$ was considered statistically significant.

Results

Effects of the temporal gradient of WSS (τ') on the structural changes (diameter and IMT) of venous wall for six AVFs with curved (C-AVF; $n = 3$) and straight (S-AVF; $n = 3$) configurations are discussed. Results are presented as mean $\pm$ SD.

Remodeling of C-AVF and S-AVF over Time

Temporal changes in anatomy and WSS of a C-AVF and S-AVF placed in the same animal are shown in Fig. 4. This figure qualitatively shows how different surgical configurations of AVFs can affect the hemodynamics and consequently, the remodeling behavior over time. Dashed lines in Fig. 4 specify similar regions (in terms of distance from the arteriovenous anastomosis) in the venous segments of C-AVF and S-AVF at all the postsurgery time points. It should be noted that the WSS values in Fig. 4 corresponded to the local time-averaged WSS magnitude at each boundary node and not the axial temporal and spatial averaged WSS values as presented in the rest of this article.

At 2D, WSS levels for the C-AVF in the specified region were lower as compared with those for S-AVF. In particular, WSS levels at the region specified by the "*" symbol for S-AVF were almost five times greater than those for C-AVF. Further at 7D, although WSS levels decreased in both AVFs, the luminal dilation for C-AVF was considerably greater than S-AVF. Comparison between the regions specified by the "*" symbol for S-AVF at 2D and 7D shows that this area dilated at 7D as WSS decreased to almost half of its value at 2D. By 28D, however, there was a significant increase in luminal diameter of the C-AVF. In contrast, the venous segment of the S-AVF became stenosed. WSS for C-AVF at 28D had similar levels as those at 7D, while WSS for S-AVF at 28D was significantly higher than the corresponding levels at 7D. For S-AVF, the areas with the highest WSS occurred in the regions with severe stenosis.

Quantifying the Changes in Luminal Diameter of C-AVF and S-AVF over Time

As the venous luminal cross-sections do not form a circle during the remodeling process, hydraulic diameter (D_h) of the venous' cross-sections was calculated. D_h was defined as the ratio of cross-sectional area (A) to the wetted perimeter (P) as shown in Eq. 1:

$$D_h = 4\frac{A}{P} \tag{1}$$

Mean D_h of the venous segment at the postsurgery time points is shown for C-AVF and S-AVF in Fig 5A.

TABLE 1. Data Matrix: Pig 1 was sacrificed at 7D postsurgery, while pigs 2 and 3 were sacrificed 28D after AVF placement. (CT, US, and His stand for CT scan, ultrasound, and histology analysis, respectively)

		2D (D: days)			7D				28D			
		CT	US*	CFD	CT	US*	CFD	His	CT	US*	CFD	His
Pig 1	C-AVF	✔	✔	✔	✔	✔	✔	✔				
	No. of data		4			4		4				
	S-AVF	✔	✔	✔	✔	✔	✔	✔				
	No. of data		4			4		4				
Pig 2	C-AVF	✔	✔	✔	✔	✔	✔		✔	✔	✔	✔
	No. of data		4			4				4		4
	S-AVF	✔	✔	✔	✔	✔	✔		✔	✔	✔	✔
	No. of data		4			4				4		4
Pig 3	C-AVF	✔	✔	✔	✔	✔	✔		✔	✔	✔	✔
	No. of data		4			4				4		4
	S-AVF	✔	✔	✔	✔	✔	✔		✔	✔	✔	✔
	No. of data		4			4				4		4

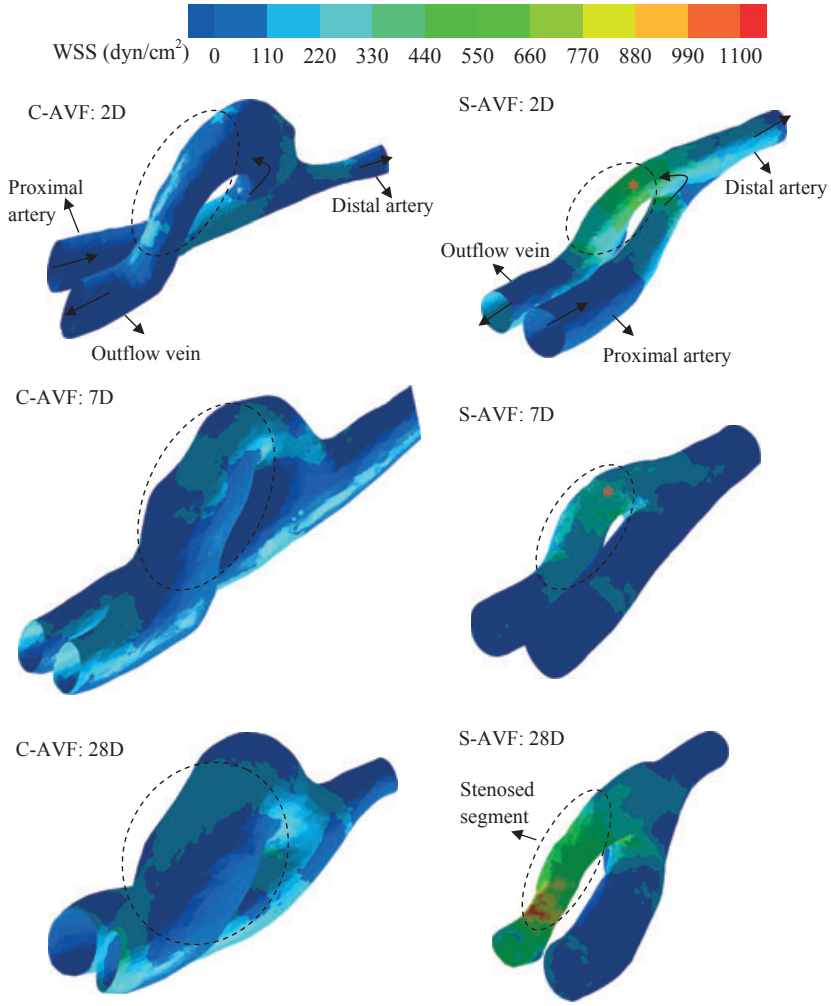

FIG. 4. Variation in anatomy and WSS within a C-AVF (left) and S-AVF (right) placed in the same pig at all the postsurgery time points (see text for details). Note the very significant differences in WSS between the different configurations at different time points. Note also how these changes in WSS appear to translate into differences in diameter, particularly at the later 28 day time point.

For C-AVF, D_h consistently increased from 5.68 ± 0.97 mm at 2D to 7.53 ± 0.97 mm at 7D, and to 9.66 ± 0.98 mm at 28D. For S-AVF, despite the increase in D_h from 2D (5.20 ± 0.16 mm) to 7D (6.10 ± 0.16 mm), there was a minimal increase in D_h at 28D (6.39 ± 0.18 mm). The mean D_h of C-AVF and S-AVF was not significantly different at 2D and 7D, while at 28D, the difference became significant ($p < 0.05$).

In addition to the magnitude of D_h, changes in the luminal diameter of AVFs between sequential time points ($\Delta D_h = [D_{h\ (28D\ or\ 7D)} - D_{h\ (7D\ or\ 2D)}]$) were calculated for both configurations. For C-AVF and S-AVF, ΔD_h measured between 2D and 7D, as well as between 7D and 28D, is shown in Fig. 5B. Between 7D and 2D, ΔD_h for C-AVF and S-AVF was 1.79 ± 0.57 mm and 0.60 ± 0.42 mm, respectively. During this period, the difference between the mean ΔD_h between the two configurations was marginally significant ($p = 0.1$). However, between 28D and 7D, ΔD_h for C-AVF was 2.27 ± 0.67 mm and significantly greater ($p < 0.05$) than the relatively small ΔD_h (= 0.02 ± 0.55 mm) for S-AVF.

Changes in IMT over Time for Different Configurations of AVF

Overall mean of IMT averaged in both configurations at 7D and 28D is shown in Fig. 6A. IMT was 35.39 ± 9.89 units at 7D, which almost doubled by 28D (= 70.86 ± 7.04 units). The difference between the amount of IMT at 7D and 28D was significant ($p < 0.05$). The amount of IMT for C-AVF and S-AVF at 7D and 28D is shown in Fig 6B. At 7D, IMT was 38.94 ± 9.91 units and 25.81 ± 11.61 units for C-AVF and S-AVF, respectively. The difference between IMT at 7D was not statistically significant between the configurations. At 28D, IMT almost doubled in both configurations (C-AVF: 77.46 ± 7.10 units and S-AVF: 53.71 ± 8.23 units) and interestingly, the difference between IMT of the two groups was found to be significant ($p < 0.05$).

Effect of Different Configurations of AVF on Venous' Hemodynamics over Time

Changes in the WSS levels of the two configurations at all postsurgery time points are shown in Fig. 7A. For

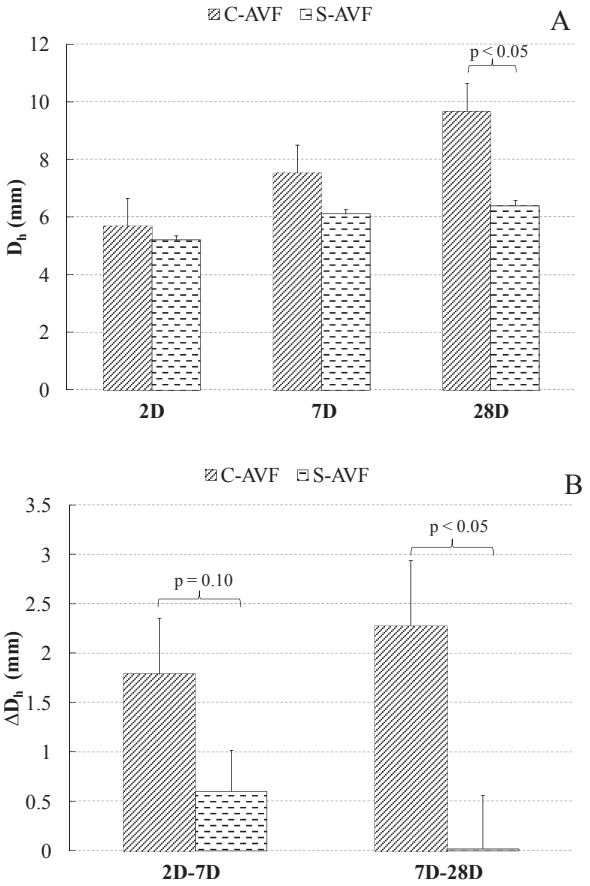

FIG. 5. (A) Hydraulic diameter of outflow vein over time and (B) changes in hydraulic diameter of venous segment for C-AVF and S-AVF.

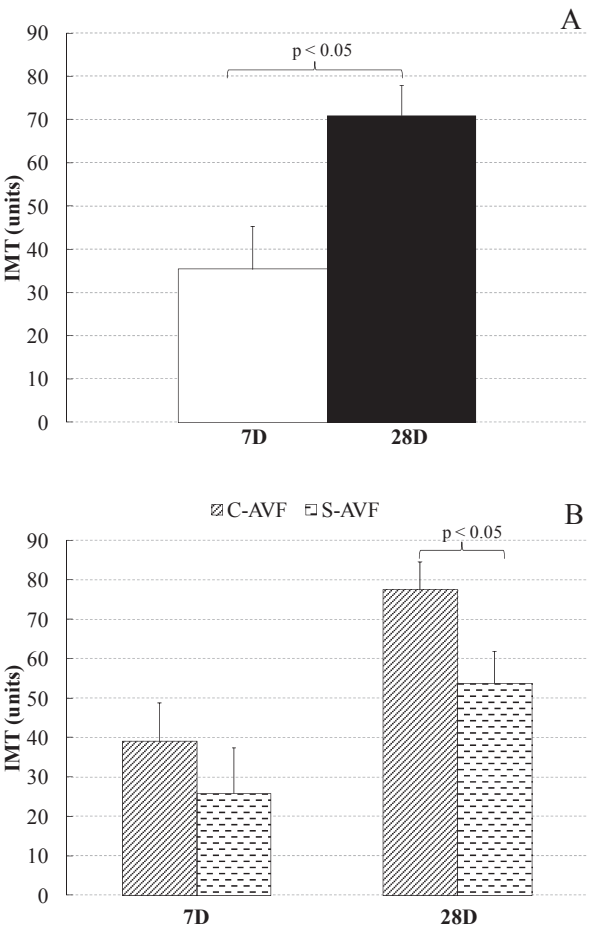

FIG. 6. (A) Overall mean of IMT at 7D and 28D and (B) IMT of C-AVF and S-AVF at 7D and 28D.

C-AVF, WSS decreased consistently over time (2D: 22.29 ± 4.77 dyne/cm^2, 7D: 16.93 ± 4.77 dyne/cm^2, 28D: 4.08 ± 5.08 dyne/cm^2), while for S-AVF, WSS increased from 2D (13.02 ± 5.01 dyne/cm^2) to 7D (20.42 ± 5.01 dyne/cm^2), and to 28D (36.68 ± 5.32 dyne/cm^2), which was almost nine times greater than the corresponding WSS for C-AVF. The difference among the levels of WSS between the two configurations was not significant at 2D and 7D; however, it achieved significance at 28D.

In addition to the absolute levels of WSS over time, the slope of changes in WSS levels between the successive time points $\left(\tau' = \frac{WSS_{28D} - WSS_{7D}}{\Delta time} \quad \text{and} \quad \tau' = \frac{WSS_{7D} - WSS_{2D}}{\Delta time}\right)$ was also studied (Fig. 7B). For C-AVF, τ' was negative between all the successive time points (between 7D and 2D: $\tau' = -1.47 \pm 0.60$ dyne/cm^2/day; between 28D and 7D: $\tau' = -0.56 \pm 0.60$ dyne/cm^2/day), which shows the reduction in WSS levels over time. However, for S-AVF, τ' had positive values of 1.82 ± 0.39 dyne/cm^2/day between 7D and 2D and 0.71 ± 0.39 dyne/cm^2/day between 28D and 7D, which show a consistent increase in WSS levels over time. The difference between the τ' of the two configurations was significant ($p < 0.05$) from 2D to 7D, while it was moderately significant ($p = 0.07$) from 7D to 28D.

Effect of τ' on AVF Remodeling

Vascular remodeling represents structural changes in diameter and thickness of vessels as a response to changes in the hemodynamic environments. In Figs 8A and 8B, the effect of τ' on ΔD_h and IMT of C-AVF and S-AVF are shown, respectively. Here, τ' represents the changes in the hemodynamics of the AVF, while ΔD_h and IMT embody the structural changes in the venous segment. *In addition, the effect of τ' on a new nondimensional parameter, ΔD_h/IMT, which combines the effects of ΔD_h and IMT, was also studied* (Fig 8C). In these figures, τ' values have been described only for the changes in WSS between 7D and 28D as the differences in ΔD_h and IMT between the two configurations were significant only between 7D and 28D (Figs 5B and 6B).

For C-AVF, as shown in Fig. 8A, ΔD_h has a significant ($r = 0.67$) direct correlation with τ', while ΔD_h and τ' showed an inverse relationship ($r = -0.77$) for S-AVF. The τ' was negative for C-AVF and the largest ΔD_h values corresponded to smallest negative levels of τ'. In contrast, S-AVF has both negative and positive levels of τ'. The negative levels of τ' for S-AVF had similar values of ΔD_h as for C-AVF, while regions with positive τ' were associated with the smallest values of ΔD_h.

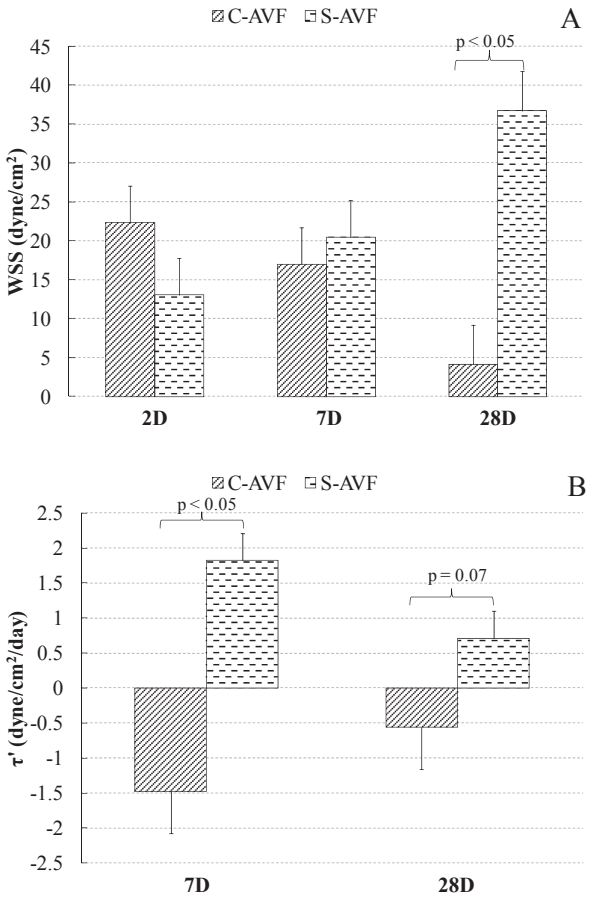

FIG. 7. (A) Variation in WSS levels and (B) temporal gradient of WSS over time for C-AVF and S-AVF.

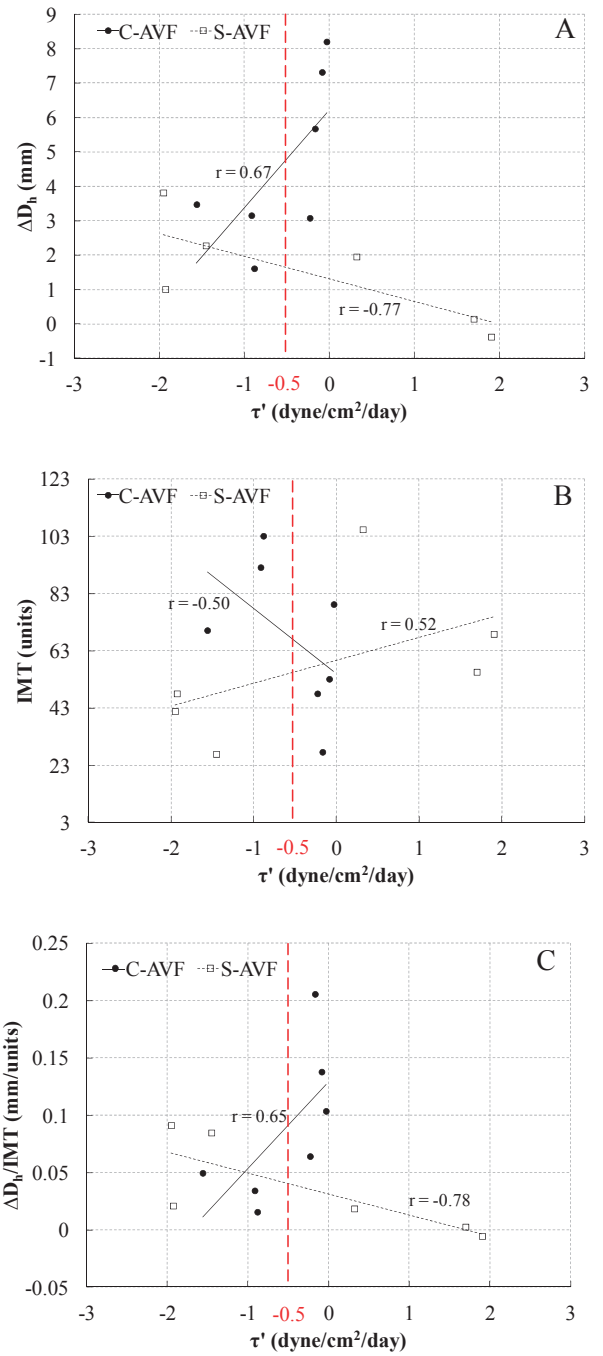

FIG. 8. Variation in (A) changes in luminal diameter, (B) IMT, and (C) ΔD_h/IMT with respect to τ' for C-AVF and S-AVF.

Moreover, τ' showed significant inverse correlation with IMT ($r = -0.50$) for C-AVF, while it had a significant direct relationship with IMT ($r = 0.52$) for S-AVF. For C-AVF, regions with the largest negative levels of τ' were associated with the largest amount of IMT. However, the largest amount of IMT for S-AVF occurred in regions with positive levels of τ'.

Furthermore, τ' showed a significant correlation with the combined effects of ΔD_h and IMT, introduced as a nondimensional parameter: ΔD_h/IMT. A direct relationship ($r = 0.65$) was found between ΔD_h/IMT and τ' for C-AVF, which shows that the regions with smaller negative levels of τ' had larger positive values of ΔD_h/IMT. In contrast, an inverse relationship ($r = -0.78$) was observed between ΔD_h/IMT and τ' for S-AVF, which shows that the smallest positive or negative values of ΔD_h/IMT were corresponded to positive levels of τ'.

As an example, a τ' level of -0.5 dyne/cm^2/day (specified by the vertical dashed line in Figs 8A–C) for a C-AVF was associated with a reduction in WSS levels from 15.5 dyne/cm^2 at 7D to 5 dyne/cm^2 at 28D ($\tau' = -0.5 = [5–15.5]/[28–7]$). However, for an S-AVF, WSS reduced from 33 dyne/cm^2 at 7D to 22.5 dyne/cm^2 at 28D. For this level of τ', C-AVF had larger ΔD_h (= 4.8 mm), IMT (= 68 units), and ΔD_h/IMT (= 0.08 mm/units) as compared with S-AVF (ΔD_h = 1.6 mm, IMT = 58 units, and ΔD_h/IMT = 0.04 mm/units).

Discussion

The effect of temporal gradient of WSS (τ') on the venous wall remodeling characterized by changes in the luminal diameter and wall thickness was studied in AVFs with two different configurations. The *major findings* of this research can be summarized as (a) *surgical*

configuration of AVF has a strong impact on hemodynamic shear stress profiles within an AVF and ultimately, on the histological endpoints (IMT); (b) τ' was found to be an important hemodynamic factor that influences the changes in luminal diameter and IMT of venous segment in AVFs.

Surgical Configuration of AVFs

AVFs were created in two different surgical configurations with two extreme radii of curvatures referred to as curved (C-AVF) and straight (S-AVF). The C-AVFs were created with significantly larger radius of curvature as compared with S-AVFs (4.21 ± 0.31 mm vs. 2.70 ± 0.08 mm; $p < 0.05$). During the surgery, curvatures of the AVFs were mainly subjected to visual confirmation. Although minimal differences in the geometrical characteristics of AVFs such as radius of curvature and anastomosis angle were inevitable, a single surgeon placed all the AVFs to eliminate possible operator-dependent variations. In our recent work, we showed that the changes in radius of curvature of C-AVFs and S-AVFs over time were at maximum around 8% (20). Therefore, radius of curvature was the leading difference between two groups at all the time points.

Time Course of Remodeling

A week after surgery, remodeling in the form of changes in luminal diameter and IMT was observed in both groups. During this time, WSS levels for C-AVF decreased (negative τ'), while it increased for S-AVF (positive τ'). In addition, the venous diameter increased in both groups with some amount of IMT. However, none of these changes were significantly different in the two groups during the early time points (2D and 7D). Thus, after a week, both configurations underwent outward hypertrophic remodeling. It is noteworthy that despite the different temporal patterns of WSS, similar remodeling was observed in both groups.

A month after creation of AVFs, WSS levels of C-AVF decreased (negative τ') to its physiological range ($\sim$4 dyne/cm^2), which was accompanied by considerable dilation. However, WSS levels increased (positive τ') for S-AVF and remained noticeably high ($\sim$36 dyne/cm^2) with negligible change in luminal diameter. During this period, IMT doubled in both configurations as compared with IMT at 7D. This shows that venous thickening is a dynamic process and thus, the direction of growth is important as it could affect the changes in luminal diameter. Thus, IMT, when combined with outward remodeling (dilatation), results in an increase in venous diameter. Alternatively, when IMT is combined with inward remodeling, the result is venous stenosis. To determine the direction of wall growth, changes in luminal diameter (ΔD_h) of AVFs were studied. For C-AVF, ΔD_h was positive ($\sim$2.3 mm), while it was minimal ($\sim$0.02 mm) and, in some cases, negative for S-AVF. Therefore, it can be concluded that IMT occurred in combination with outward remodeling (dilation) for C-AVF, while IMT was combined with inward remodeling (constriction) for S-AVF, which then resulted in the formation of venous stenosis. Therefore, from 7D to 28D, different remodeling processes occurred in the two groups; *outward hypertrophic* remodeling for C-AVF and *inward hypertrophic* remodeling for S-AVF. It is noteworthy that in contrast to the first week, different hemodynamic and remodeling processes occurred during 7D to 28D.

Effect of τ' on Remodeling

In this study, for the first time, we demonstrated that the gradient of WSS over time is an important factor, which determines structural changes in the venous segment of AVFs. Thus, τ' had a strong correlation with venous wall thickness and dilation assessed by IMT and ΔD_h, respectively. Negative τ' was associated with large ΔD_h and favorable IMT leading to positive remodeling, while positive τ' was accompanied by relatively small or even negative ΔD_h and detrimental IMT causing adverse remodeling. Although knowledge of ΔD_h and IMT is necessary to evaluate the maturation status of AVFs, their combined effect as described by the new parameter ΔD_h/IMT could provide more insight into the remodeling patterns of AVFs. In brief, ΔD_h/IMT is a new nondimensional parameter, which describes venous dilation corrected for the amount of intima-media thickness. In general, positive values of ΔD_h/IMT are associated with luminal dilation and an outward growth of venous wall, while negative values are associated with vasoconstriction and an inward growth of venous wall.

From a clinical perspective, we have previously documented that differences in the surgical configuration of AVFs (increasing the radius of curvature of AVFs) can have a positive impact on AVF dilation and blood flow (20). We demonstrate herein that monitoring the variations in WSS over time could provide us with a handle on important structural parameters such as luminal dilation, venous wall thickening (IMT), and also the linkage between changes in diameter to venous wall thickness. Thus, τ' could perhaps be evaluated in future clinical studies as a measure and probably a predictor for clinical AVF maturation, and attempts to identify the optimal AVF configuration could perhaps focus on being able to generate that surgical configuration which optimizes values for τ' and consequently impacts upon both ΔD_h and ΔD_h/IMT in a positive fashion. This research obviously needs to be done in conjunction with the investigation/modulation of other pathways such as pressure, uremia, inflammation, and oxidative stress.

One of the limitations of this study was the relatively small sample size of the study, which is often the case in large animal experiments; however, taking multiple blocks and cross-sectional records for each AVF resulted in 16 data points (four at each histology block), which, when measured repeatedly over time, provided adequate degrees of freedom to allow statistical inferences to be made. It is noteworthy that despite the sample size, the differences between the levels of ΔD_h, IMT, and ΔD_h/IMT for the two surgical configurations were significant. Also, correlations of remodeling factors with τ' were significantly different, following distinct patterns (negative vs. positive slopes) for the two groups.

Another limitation of this study was the collapse of venous segments once dissected out postsurgery. This made it difficult to compare the local ex vivo histology data with in vivo hemodynamic parameters in the same region. To address this issue, radiopaque markers were used to orient the histological specimens correctly, while the vein shrinkage factor (defined as the ratio of AVF length before and after embedding process) was employed to find the approximate in vivo location of histology blocks. This allowed us to correlate the longitudinal changes in WSS at different regions with the corresponding IMT data.

Conclusion

We have demonstrated for the first time that different surgical configurations of AVF are probably associated with different patterns of vascular remodeling due to the generation of different longitudinal patterns of WSS. Thus, τ' was shown to have a strong linkage with geometric factors ΔD_h, IMT, and ΔD_h/IMT. Reduction in WSS levels over time represented by negative τ' were associated with large ΔD_h, favorable IMT, and positive ΔD_h/IMT (clinically, this would probably manifest as successful AVF maturation), while increase in WSS levels over time (positive τ') was accompanied by relatively small ΔD_h and detrimental IMT, and very small or negative values of ΔD_h/IMT (clinically, this would probably manifest as a failure of AVF maturation). The former represents a positive remodeling, which occurred for C-AVF, while the latter describes adverse remodeling as happened for S-AVF. Thus, C-AVF underwent outward hypertrophic remodeling as its venous luminal diameter consistently increased over time and the venous wall thickened in an outward direction. In contrast, S-AVF underwent inward hypertrophic remodeling as changes in its diameter were minimal over time and IMT growth was in an inward direction which contributed to formation of stenosis in the venous segment.

Finally, from the clinical standpoint, this study suggests that optimizing surgical configuration to achieve the right pattern of τ', ΔD_h, IMT, and ΔD_h/IMT could result in long-term AVF success. An alternative approach would be to individualize clinical AVF configurations using hemodynamic modeling that results in optimal trends for the above parameters, and then placing the modeled configuration in patients who require an AVF.

Acknowledgments

This work was funded by a VA Merit Review to Dr Roy-Chaudhury.

Conflict of Interest

The authors declare that they have no competing interests.

References

1. Herity NA, Ward MR, Lo S, Yeung AC: Review: clinical aspects of vascular remodeling. *J Cardiovasc Electrophysiol* 10:1016–1024, 1999
2. London GM, Marchais SJ, Guerin AP, Metivier F, Adda H: Arterial structure and function in end-stage renal disease. *Nephrol Dial Transplant* 17:1713–1724, 2002
3. Asif A, Roy-Chaudhury P, Beathard GA: Early arteriovenous fistula failure: a logical proposal for when and how to intervene. *Clin J Am Soc Nephrol* 1:332–339, 2006
4. Rotmans JI, Velema E, Verhagen HJM, Blankensteijn JD, Kastelein JJP, de Kleijn DPV, Yo M, Pasterkamp G, Stroes ESG: Rapid, arteriovenous graft failure due to intimal hyperplasia: a porcine, bilateral, carotid arteriovenous graft model. *J Surg Res* 113:161–171, 2003
5. Roy-Chaudhury P, Arend L, Zhang J, Krishnamoorthy M, Wang Y, Banerjee R, Samaha A, Munda R: Neointimal hyperplasia in early arteriovenous fistula failure. *Am J Kid Dis* 50:782–790, 2007
6. Roy-Chaudhury P, Lee TC: Vascular stenosis: biology and interventions. *Curr Opin Nephrol Hypertens* 16:516–522, 2007
7. Roy-Chaudhury P, Sukhatme VP, Cheung AK: Hemodialysis vascular access dysfunction: a cellular and molecular viewpoint. *J Am Soc Nephrol* 17:1112–1127, 2006
8. Friedman MH, Deters OJ, Bargeron CB, Hutchins GM, Mark FF: Shear-dependent thickening of the human arterial intima. *Atherosclerosis* 60:161–171, 1986
9. Krishnamoorthy MK, Banerjee RK, Wang Y, Zhang J, Roy AS, Khoury SF, Arend LJ, Rudich S, Roy-Chaudhury P: Hemodynamic wall shear stress profiles influence the magnitude and pattern of stenosis in a pig AV fistula. *Kidney Int* 74:1410–1419, 2008
10. Malik J, Tuka V, Tesar V: Local hemodynamics of the vascular access for hemodialysis. *Kidney Blood Press Res* 32:59–66, 2009
11. Manos TA, Sokolis DP, Giagini AT, Davos CH, Kakisis JD, Kritharis EP, Stergiopulos N, Karayannacos PE, Tsangaris S: Local hemodynamics and intimal hyperplasia at the venous side of a porcine arteriovenous shunt. *IEEE Trans Inf Technol Biomed* 14:681–690, 2010
12. Ene-Iordache B, Remuzzi A: Disturbed flow in radial-cephalic arteriovenous fistulae for haemodialysis: low and oscillating shear stress locates the sites of stenosis. *Nephrol Dial Transplant* 27:358–368, 2011
13. Haruguchi H, Teraoka S: Intimal hyperplasia and hemodynamic factors in arterial bypass and arteriovenous grafts: a review. *J Artif Organs* 6:227–235, 2003
14. Carallo C, Irace C, Pujia A, De Franceschi MS, Crescenzo A, Motti C, Cortese C, Mattioli PL, Gnasso A: Evaluation of common carotid hemodynamic forces. Relations with wall thickening. *Hypertension* 34:217–221, 1999
15. Friedman MH, Bargeron CB, Deters OJ, Hutchins GM, Mark FF: Correlation between wall shear and intimal thickness at a coronary artery branch. *Atherosclerosis* 68:27–33, 1987
16. Glagov S, Zarins C, Giddens DP, Ku DN: Hemodynamics and atherosclerosis. Insights and perspectives gained from studies of human arteries. *Arch Pathol Lab Med* 112:1018–1031, 1988
17. Kornet L, Hoeks AP, Lambregts J, Reneman RS: In the femoral artery bifurcation, differences in mean wall shear stress within subjects are associated with different intima-media thicknesses. *Arterioscler Thromb Vasc Biol* 19:2933–2939, 1999
18. Gusic RJ, Myung R, Petko M, Gaynor JW, Gooch KJ: Shear stress and pressure modulate saphenous vein remodeling ex vivo. *J Biomech* 38:1760–1769, 2005
19. Rajabi-Jaghargh E, Krishnamoorthy M, Roy-Chaudhury P, Succop P, Wang Y, Choe A, Banerjee R: Longitudinal assessment of hemodynamic endpoints in predicting arteriovenous fistula maturation. *Semin Dial*, 2012
20. Krishnamoorthy MK, Banerjee RK, Wang Y, Choe AK, Rigger D, Roy-Chaudhury P: Anatomic configuration affects the flow rate and diameter of porcine arteriovenous fistulae. *Kidney Int* 81:745–750, 2012
21. Krishnamoorthy M, Roy-Chaudhury P, Wang Y, Sinha Roy A, Zhang J, Khoury S, Munda R, Banerjee R: Measurement of hemodynamic and anatomic parameters in a swine arteriovenous fistula model. *J Vasc Access* 9:28–34, 2008
22. Wang Y, Krishnamoorthy M, Banerjee R, Zhang J, Rudich S, Holland C, Arend L, Roy-Chaudhury P: Venous stenosis in a pig arteriovenous fistula model – anatomy, mechanisms and cellular phenotypes. *Nephrol Dial Transplant* 23:525–533, 2008
23. Niazmand H, Rajabi Jaghargh E: Bend sweep angle and reynolds number effects on hemodynamics of S-shaped arteries. *Ann Biomed Eng* 38:2817–2828, 2010
24. Banerjee RK, Cho YI, Back LH: Numerical studies of three-dimensional arterial flows in reverse curvature geometry: part I – peak flow. *J Biomech Eng* 115:316–326, 1993